Bulletin of the Seismological Society of America, Vol. 85, No. 4, pp. 1021–1038, August 1995

Moment-Tensor Inversions for Local Earthquakes Using Surface Waves Recorded at TERRAscope

by Hong Kie Thio and Hiroo Kanamori

Abstract We have developed a method to determine moment tensors for local earthquakes using short period (10 to 50 sec) surface waves recorded at TERRAscope stations. To correct for the substantial lateral variations in crustal structure, we applied phase corrections to the data using a regionalized phase-velocity model. We have determined moment tensors for over 180 events in the last 3 yr in southern California for magnitudes as small as 3.2 and as large as 6.5. The results are consistent with those obtained from first-motion data as well as other waveform inversions. When continuous data telemetry from the stations becomes available this method can yield moment tensors for earthquakes in southern California and adjacent regions within minutes after the occurrence of an event.

Our results confirm the relation log M_0 (seismic moment) $\propto 1.5M_L$ (local magnitude) obtained by an earlier study.

Introduction

With the deployment of dense digital broadband networks like TERRAscope we are now capable of carrying out rapid determinations of source parameters using a variety of methods. In this article, we present one such method, viz., moment-tensor inversion using regional surface waves. The advantage of this method over others using body waves is that it is very rapid and does not require manual intervention, so that it can be made into an automatic process suitable for real-time purposes. Real-time analysis of earthquakes can be very important, since it can help us estimate the damage after an earthquake even before reports from the field come in, potentially increasing the efficiency of rescue operations. Knowledge of the mechanism also helps us to determine on which fault the earthquake occurred, which is important for the analysis of short-term seismic hazard.

We can analyze smaller events better with surface waves since body waves, with their shorter periods, tend to be more contaminated with noise than surface waves. Surface waves have already been used successfully in the determination of source parameters of earthquakes (e.g., Aki, 1966; Mendiguren, 1977; Kanamori and Given, 1981; Dziewonski and Woodhouse, 1983; Romanowicz and Monfret, 1986; Patton, 1980). In general, they are used to study larger earthquakes since these events generate sufficiently large surface waves at longer periods. The use of shorter periods (<50 sec) was hampered by the fact that these waves are sensitive to lateral inhomogeneity in the Earth's velocity structure and are therefore difficult to model over large distances. On the other hand, local arrays that are used to study smaller earthquakes in seismically active regions usually do not have sufficiently long-period response to record even short-period surface waves. Regional broadband networks like TERRAscope (Fig. 1, Table 1) enable us to use these methods to their fullest advantage even for smaller earthquakes (Romanowicz *et al.*, 1993; Patton and Zandt, 1991; Ritsema and Lay, 1993).

Since the spring of 1992, we have a prototype of this system in operation at the Caltech Seismo Lab and we now routinely analyze events with magnitude larger than 3.2 in southern California. In this article we discuss the inversion method and its implementation; we will show results for local earthquakes and compare them with results from first-motion and body-wave studies.

Table 1
List of TERRAscope Stations. All Stations are Equiped with Streckeisen Instruments (STS-1 or STS-2) as Well as CMG-1 Strong-Motion Accelerographs.

Station	Latitude	Longitude	Type
PAS	34.148	−118.172	STS-1
GSC	35.300	−116.810	STS-1
ISA	35.643	−118.480	STS-1
PFO	33.609	−116.455	STS-1
SBC	34.442	−119.713	STS-1
BAR	32.680	−116.672	STS-1
NEE	34.823	−114.596	STS-2
MLA	37.634	−118.838	STS-2
USC	34.019	−118.286	STS-2
SVD	34.104	−117.098	STS-2
VTV	34.567	−117.333	STS-2
RPV	33.744	−118.403	STS-2
DGR	33.650	−117.009	STS-2
SNCC	33.248	−119.524	STS-1

Theory

Moment-tensor inversions using surface waves are carried out either in the frequency domain (Mendiguren, 1977; Kanamori and Given, 1981; Romanowicz and Monfret, 1986) or in the time domain (Dziewonski and Woodhouse, 1983; Kawakatsu, 1989). The latter method includes the higher modes that give additional constraints on the mechanism and especially the depth of deep events. The spectral method only uses fundamental-mode surface waves but since these dominate the waveforms this is not regarded as a severe drawback. In this case, the inverse problem becomes particularly simple and straightforward as described by Kanamori and Given (1981), henceforth to be referred to as K&G. The method we used closely follows their article and we refer to that article for the formulations and derivations. In essence, we take the complex spectrum of the surface waves at various stations, and correct them for propagation effects. We can write the corrected spectrum, $V(\theta)$, as a linear combination of the moment-tensor elements, as follows, for Rayleigh waves:

$$V_R(\omega) = -P_R\left[M_{xy}\sin 2\varphi - \frac{1}{2}(M_{yy} - M_{xx})\cos 2\varphi\right] - \frac{1}{2}S_R(M_{yy} + M_{xx}) + iQ_R(M_{yz}\sin\varphi + M_{xz}\cos\varphi), \quad \text{(K\&G, equation 5)}$$

and for Love waves:

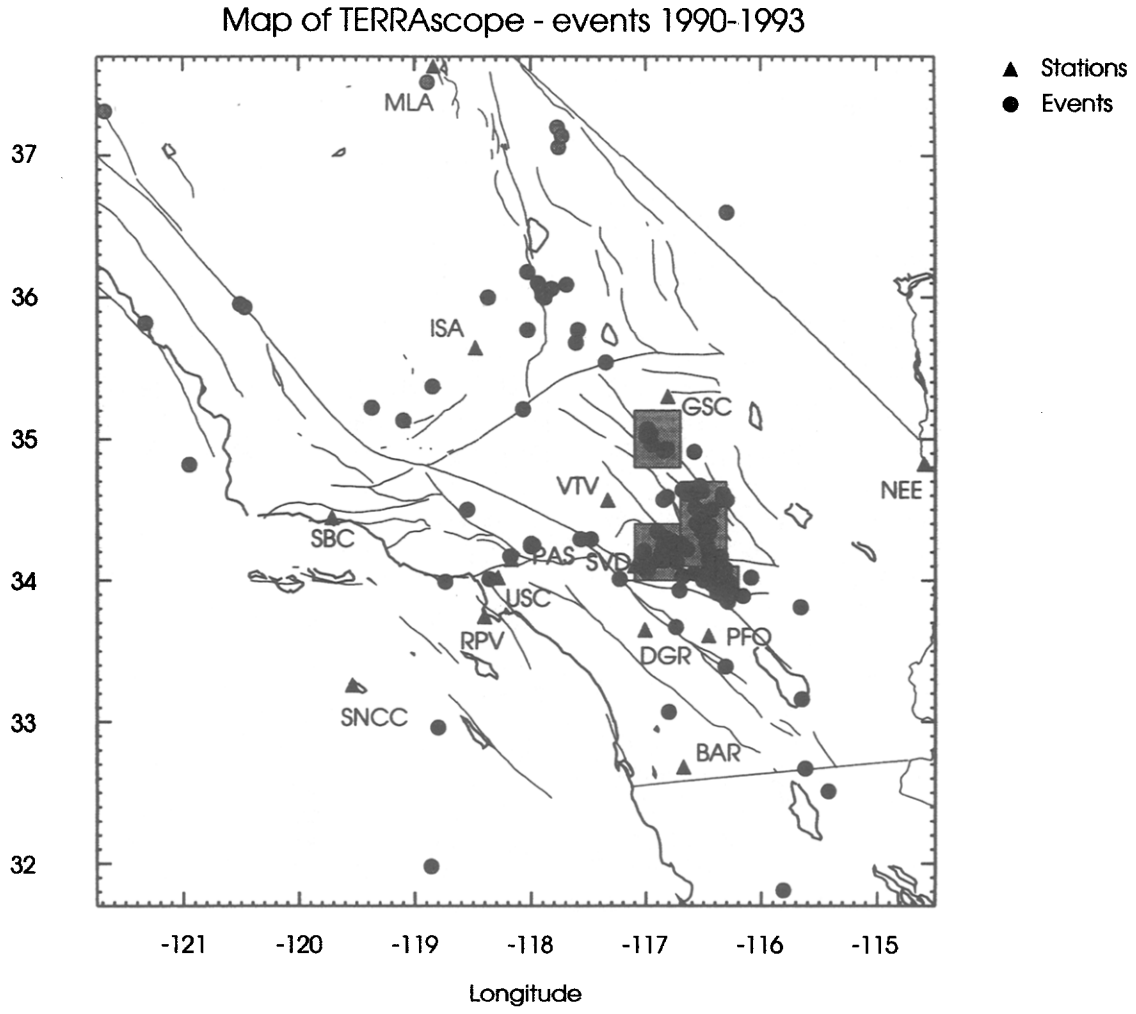

Figure 1. Map of southern California with the location of events included in this study and the stations of the TERRAscope network. The shaded blocks represent aftershock zones of the 1992 Joshua Tree and Landers–Big Bear earthquakes and are blown up in Figures 11 and 12.

$$V_L(\omega) = P_L\left[\frac{1}{2}(M_{xx} - M_{yy}) \sin 2\varphi - M_{xy} \cos 2\varphi\right]$$

$$+ iQ_L[-M_{xz} \sin \varphi + M_{yz} \cos \varphi].$$

(K&G, equation 14)

The terms $V_{L,R}$ are the corrected spectra (at the source), $P_{L,R}$, $Q_{L,R}$, S_R are the excitation functions (see also Fig. 2), and φ the azimuth to the station measured from the fault strike. We obtain the moment-tensor by solving the following:

$$\mathbf{Am} = \mathbf{v} \quad \text{(K\&G, equation 7)}$$

in the least-squares sense. Here, **A** is a matrix containing the excitation functions and the azimuthal (φ) terms, for the different frequencies, **m** is a vector containing the moment tensor elements M_{ij}, and **v** a vector containing the real and imaginary parts of the spectral data, $V_{L,R}$.

To reduce the noise, both instrumental and from higher modes, we apply a group-velocity window (between 2.5 and 4.5 km/sec) to the data before the Fourier transformation. In the frequency domain, we then pick the spectrum at four or five periods between 10 and 50 sec for the inversion. At periods shorter than 10 sec the influence of lateral inhomogeneity and body-wave phases becomes too large. For small events there is very little energy at periods longer than 30 sec so that for routine purposes we use this period interval. However, if the need arises in case of a large event, we can always extend this period range upward.

This method is valid if the source dimension and duration are small compared with the epicentral distance and the period of the surface wave, respectively. The source duration for events smaller than $M_W = 6$ is usually much smaller than the periods of the surface waves used in this inversion; we use a duration of 1 sec for routine processing. For larger events we can either increase the source duration or the periods we use. If the source dimensions become very large, simple time corrections are not valid anymore and we would have to take directivity effects into account as well. If the stations are very close to the earthquake, the point-source approximation is also violated but including finite rupture dimensions would necessitate some major changes of the method.

Although it is evident that there is strong lateral inhomogeneity in southern California, we use a single set of eigenfunctions to calculate the excitation functions. Changes in velocity model have only second-order effects on the eigenfunctions; the lateral inhomogeneity, as we shall see later, is concentrated in the upper 4 to 5 km of the crust, whereas many earthquakes occur at larger depths. In Fig. 2 we present excitation functions calculated for three crustal models (Fig. 3), which are only different from each other in the upper 3 km. It is clear that for events at a depth of 10 km the difference is marginal, especially at periods longer than 15 sec, whereas for a depth of 3 km the difference in amplitude is more substantial. However, the shape of the excitation functions and the location of the zero crossings, which are important in determining the mechanisms and depth, are not very different for any depth. Therefore, we only expect the moment for shallow events to be influenced by our use of a single crustal model. This conclusion has been substantiated by running some inversions with the different crustal models.

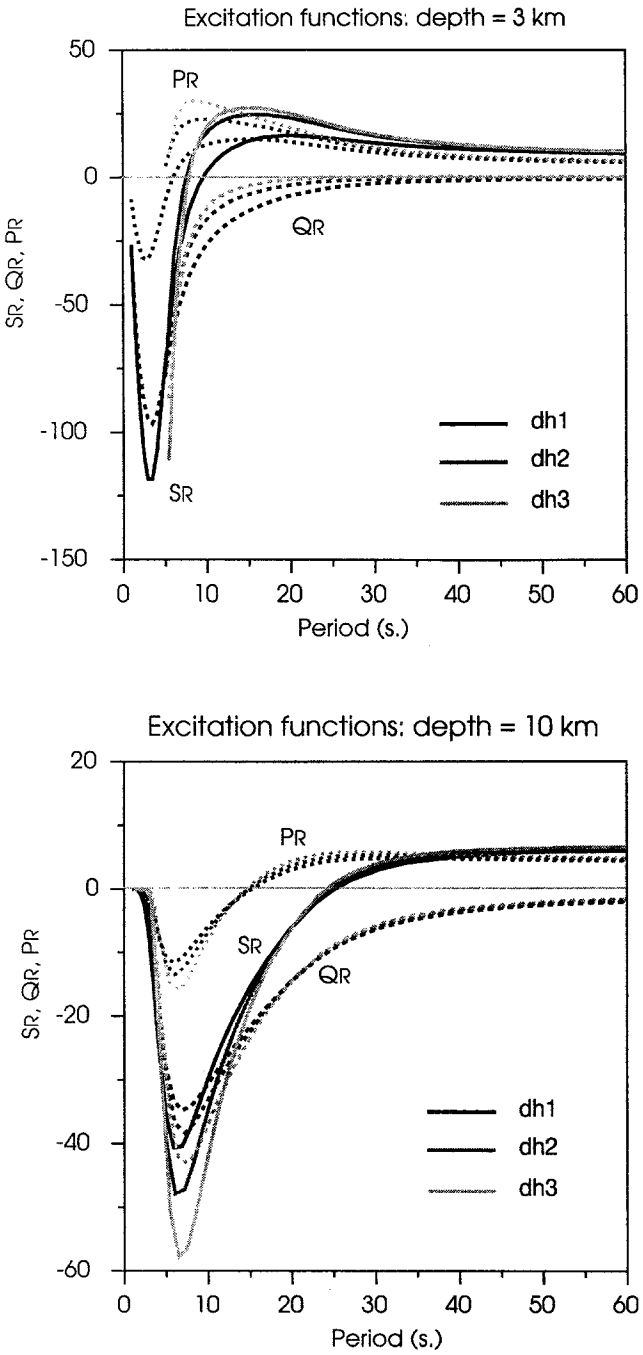

Figure 2. Rayleigh-wave excitation functions calculated for three velocity models (Fig. 3). The functions have been calculated for (a) a depth of 3 km and (b) a depth of 10 km.

On the other hand, the phase velocities are very different for the three different crustal structures (Fig. 4) and we therefore have to include a phase correction based on a laterally inhomogeneous (phase) velocity model.

Velocity Model

We constructed a preliminary velocity model for southern California by analyzing some of the larger local events for which well-constrained mechanism solutions are available. We calculated the source phase for these events and subtracted it from the phase of the surface waves at the stations. The phase velocity was then determined by using

$$c(T) = \frac{\Delta}{(\varphi_1 - \varphi_s + 2n\pi)T},$$

where T is the period, φ_1, data phase, φ_s, the source phase,

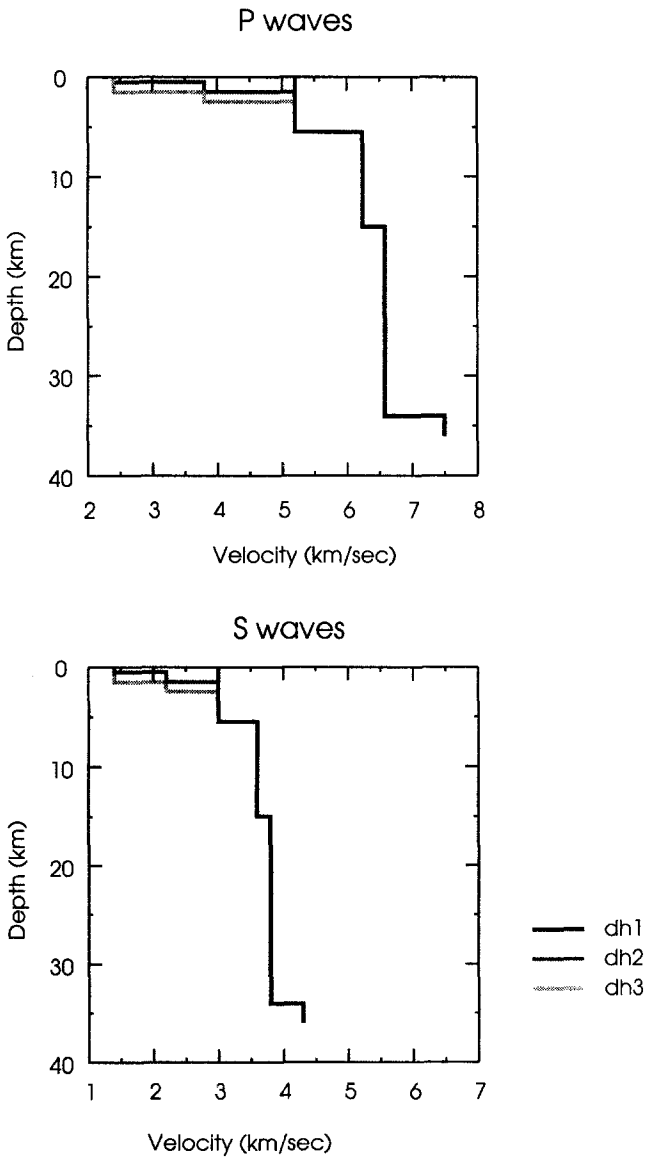

Figure 3. Velocity models [(a) P waves and (b) S waves] used to calculate the excitation functions (Fig. 2) and the dispersion curves of Figure 4. The difference between the models is in the upper 3 km where dh1 has no slow layers, whereas dh2 and dh3 have low-velocity layers with increasing thickness.

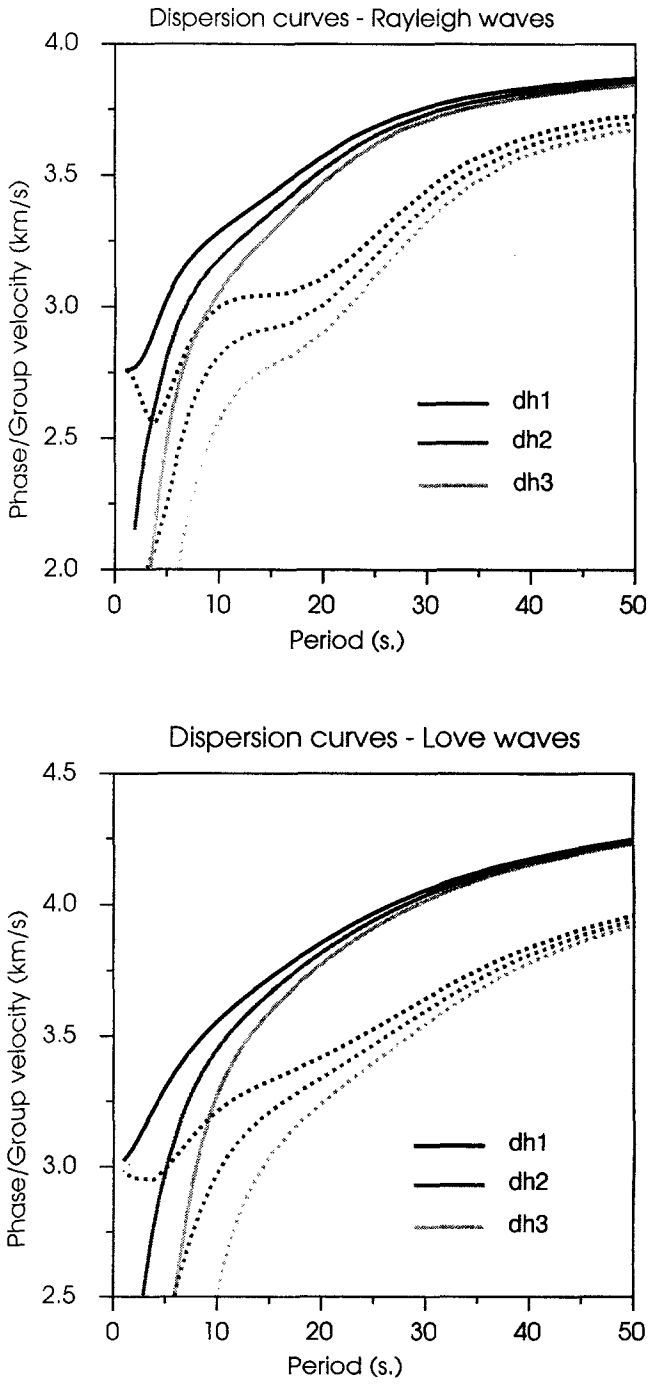

Figure 4. Dispersion curves for the velocity models in Fig. 3. Both group and phase velocity are plotted for (a) Rayleigh waves and (b) Love waves.

and n an integer. The value for n was chosen at longer periods assuming that the phase velocities determined here are close to some model phase velocities.

On the basis of the velocity curves thus obtained for every path, we divided southern California into five regions (Fig. 5) with distinct dispersion curves (Fig. 6). This regionalized model is used to correct the phase of the data for the propagation delay. An example of this correction is given in Figures 7b and 7c, which show the difference in waveform between a seismogram calculated using an average model and a seismogram that has been corrected for lateral phase-velocity variations. For areas outside these subregions we assume a generic dispersion curve based on the model used by Dreger and Helmberger (1991). From a comparison of the dispersion curves of the various paths we can see that there is a variation in phase velocity of up to 10% between the different paths. The most pronounced anomalies are in the western and northwestern areas involving paths to the Santa Barbara station (SBC) and paths from the Central Valley as well as the Sierra Nevada. The seismograms show complicated waveforms with long coda wave trains after the surface wave, which suggests that multipathing has occurred along those paths.

From the modeling of regional broadband body waves Dreger and Helmberger (1991) concluded that they can be reproduced accurately with one-dimensional models, i.e., without lateral variations. This implies that the lateral variations that we found are concentrated in the upper few kilometers of the crust for which the body waves are not very sensitive. When we calculate dispersion curves for different crustal models (Fig. 3), it is also clear that the upper 5 km have a large effect on the phase velocities (Fig. 4) in the period range from 10 to 30 sec.

Synthetic Tests

We have also carried out synthetic tests in which we calculated full waveforms using an f-k code (Saikia, personal comm.) and inverted these waveforms using our moment-tensor inversion. The results indicate that the influence of higher mode, i.e., body-wave, contamination on our results is negligible. This is also apparent from visual comparison of the full waveform synthetics and those calculated with fundamental modes only (Fig. 7), if they are low-pass filtered at 10 sec. We think that multipathing of the fundamental-mode surface waves due to lateral heterogeneity is a larger source of error than the existence of higher modes. Because the synthetic seismograms were calculated using a one-dimensional model, whereas our inversion compensates for lateral variations, we actually included some noise in

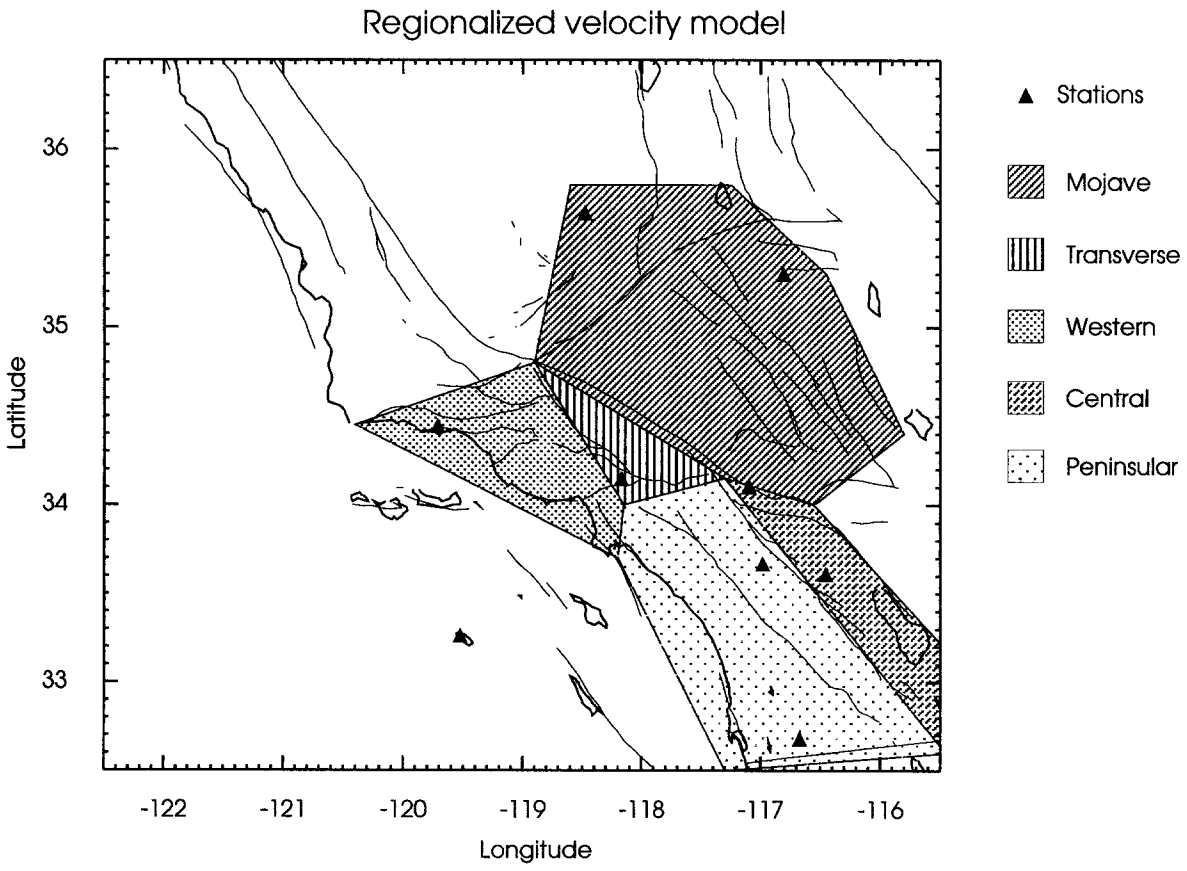

Figure 5. Regionalized velocity model for southern California. The labels correspond to the dispersion curves in Figure 6.

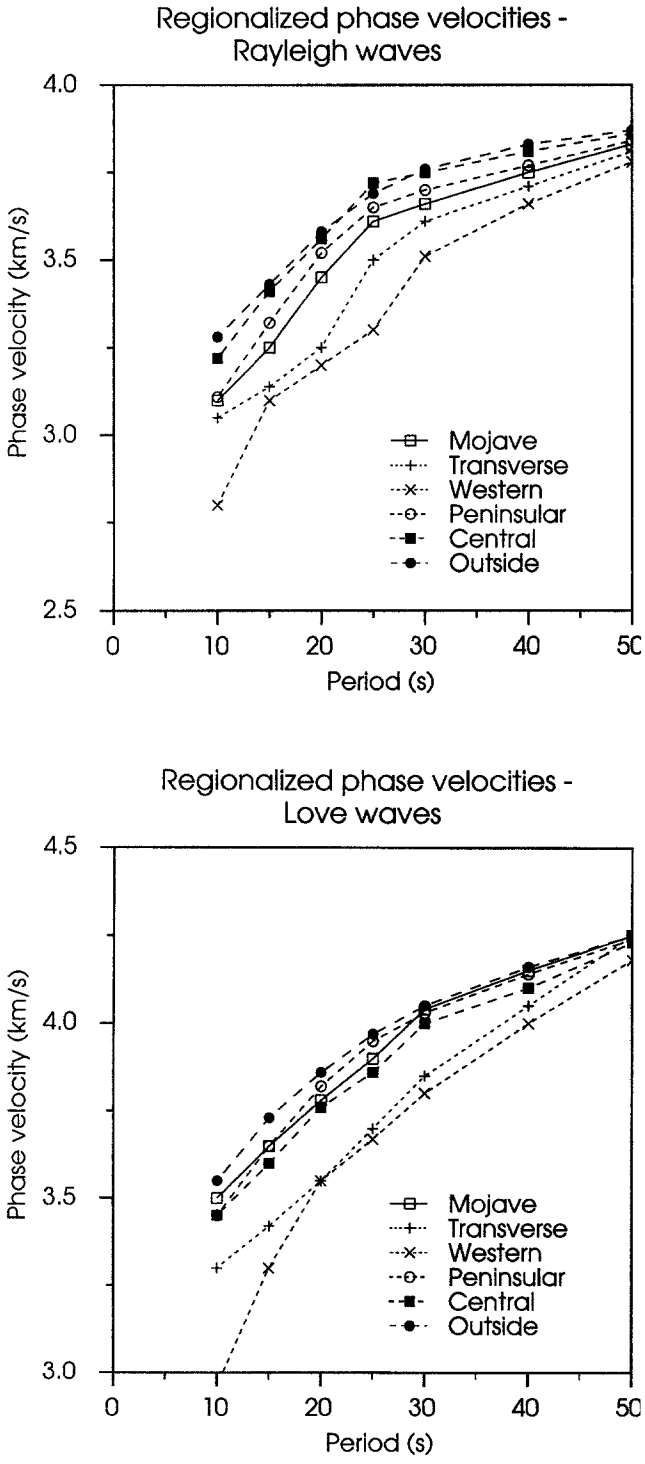

Figure 6. Dispersion curves for the different subregions. "Other" refers to areas outside these regions. These velocities have been determined using some well-constrained master events. (a) Rayleigh waves and (b) Love waves.

these tests in the form of phase errors. Nevertheless, the resulting solutions were always very close to the mechanisms for which the synthetics had been calculated with differences in strike and dip on the order of 5° and differences in depth on the order of 1 to 2 km. The best test results were obtained for events deeper than 5 km.

Depth Determination

The inversion result depends on depth (Fig. 8), and using an incorrect depth can give rise to a large non-double-couple component in the moment tensor, but it can also result in a different mechanism. This can be seen from the shape of the excitation functions for different depth (Fig. 2). The extrema and zero crossings of the excitation functions for different periods occur at different depths. Therefore, if the inversion is carried out at the wrong depth, the resulting mechanism may be very different. Since the depths obtained from the local networks are usually not well constrained, especially right after the earthquake, it is necessary to determine the depth as well. Because of the rapidity of the inversion we can determine the depth by inverting for a whole range of depths, typically between 1 and 20 km with 1-km intervals, and choosing the depth where the variance

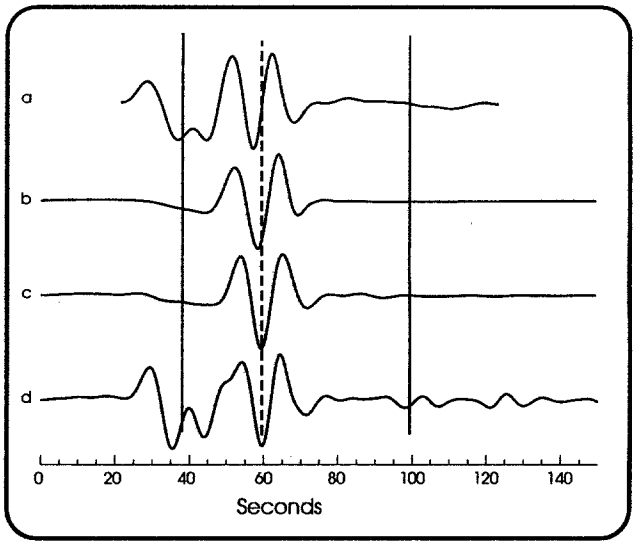

Figure 7. Comparison of data and synthetic seismograms. Seismogram (a) was calculated using an *f-k* code (Saikia, personal comm.), (b) was calculated with fundamental-mode summation, similar to the one used in the inversion, (c) is identical to (b) except that the phase velocities have been corrected using the regionalized phase-velocity model, and (d) is the actual data recorded at station PAS. All synthetic seismograms were calculated using the mechanism determined with our inversion procedure and all seismograms were bandpass filtered between 100 and 10 sec. The solid vertical lines indicate the group-velocity window that is used in the inversion. The dashed line shows the lineup of the phases.

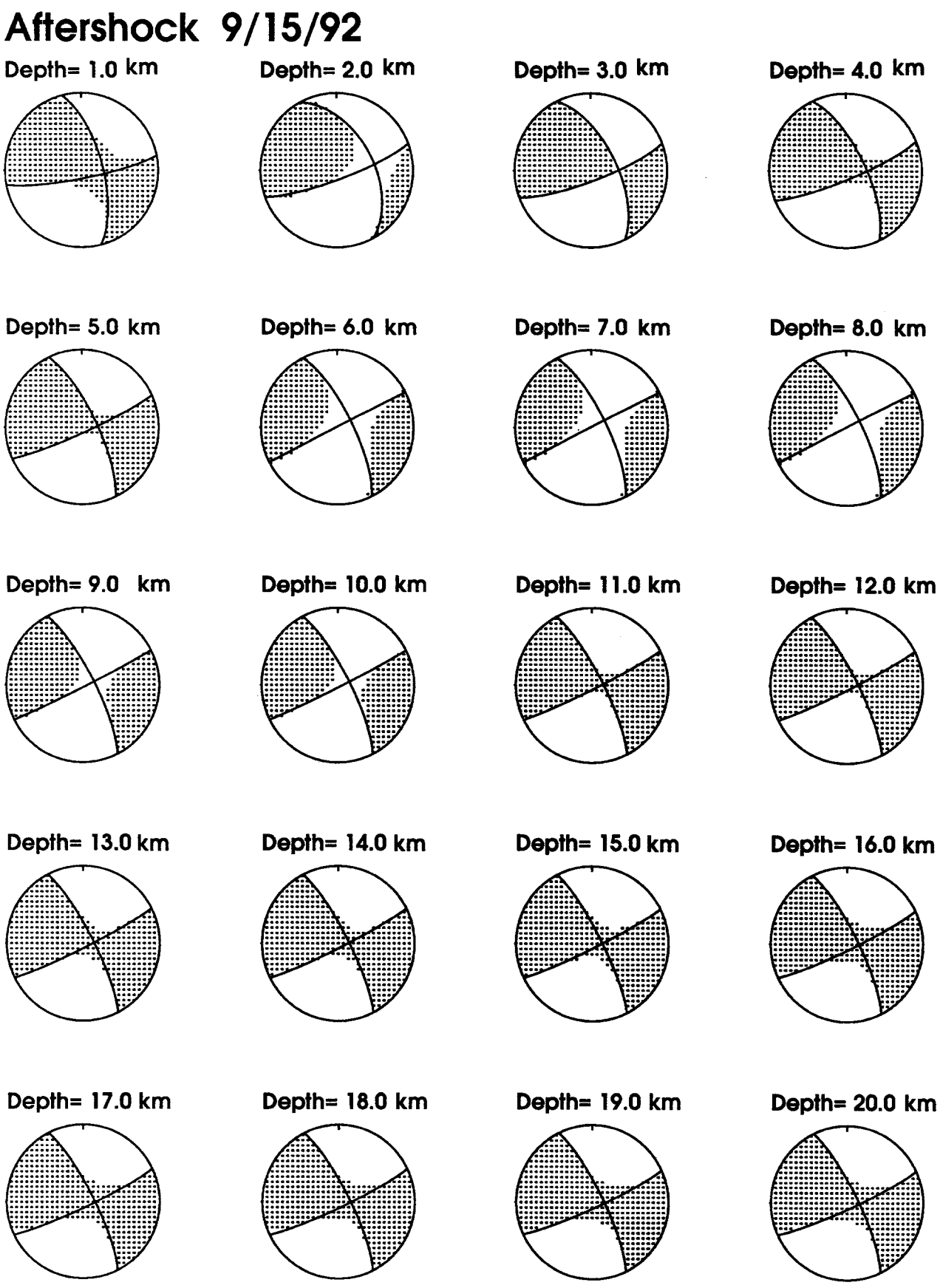

Figure 8. (a) An example of the variation of the moment-tensor solution, (b) non-double-couple component, (c) variance, and (d) moment, with depth.

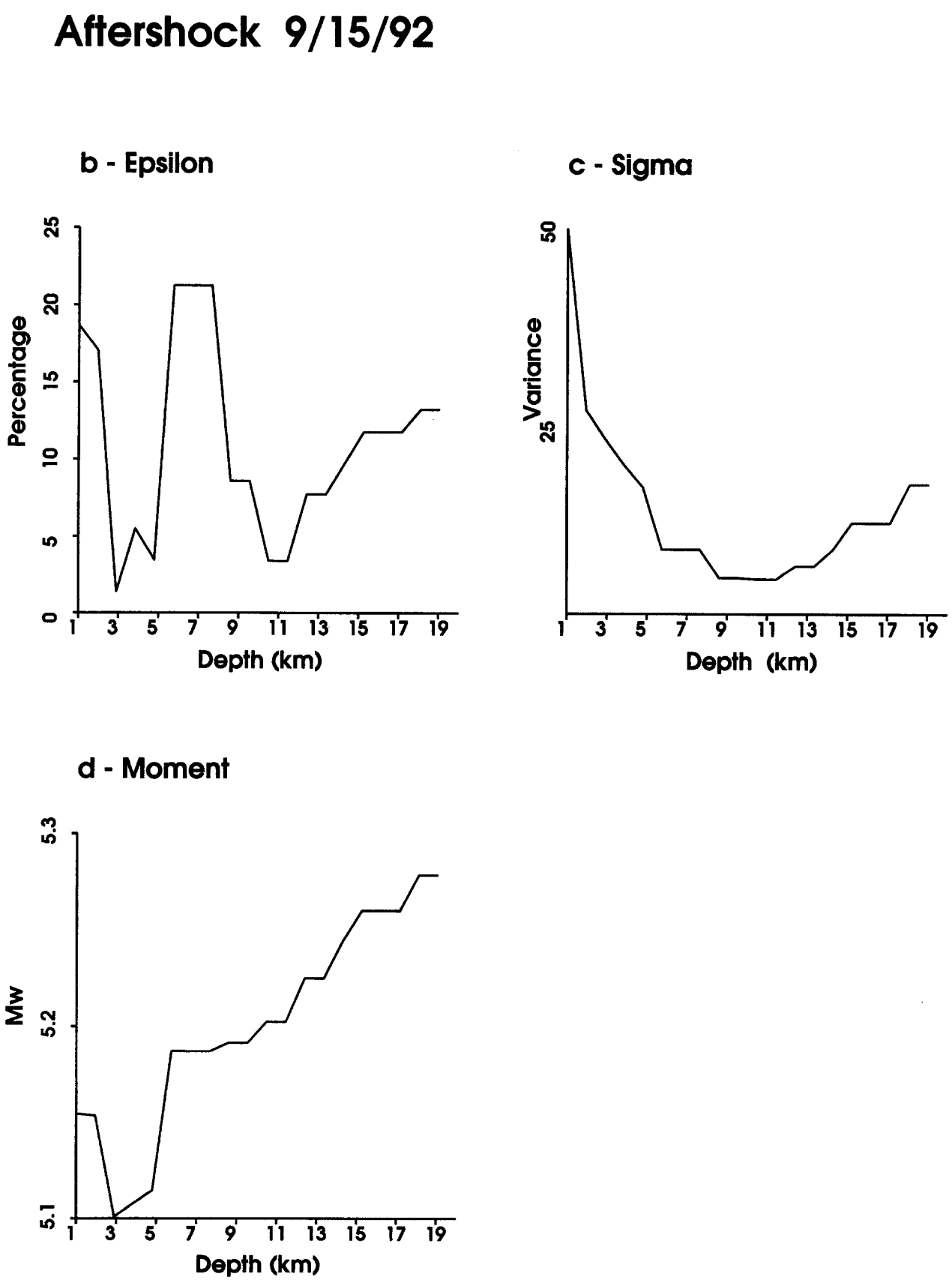

Figure 8—*Continued*

is minimal. This depth often coincides with a minimum in the nondouble component. Our depth determinations are consistent with those obtained by other methods based on waveform inversion or first-motion data, except for events shallower than 5 km. The differences for shallow events are probably the result of several factors; the first-motion solutions are unreliable for shallow events, the uppermost crust has the strongest lateral variation, so that our eigenfunctions may not be appropriate, and for shallow events the eigenfunctions in the period range we use are not very sensitive to depth. It is difficult to give an error margin for the depth determination because the width of the minimum varies from event to event, but usually the minimum in variance is well constrained within 2 km.

Performance and Results

We have used this inversion program since the spring of 1992 on a routine basis and have also studied the events recorded during the early deployment of TERRAscope. These events include the following: the 1991 Sierra Madre earthquake, the 1992 Coso swarm, and the 1992 Joshua Tree and Landers–Big Bear sequences amounting to well over 180 events ranging in magnitude from 3.2 to 6.5 (Appendix A). An example of an inversion result for a Landers aftershock is given in Figure 9. Figure 10 shows some representative moment-tensor solutions with the best-fitting double couple and the first-motion picks from the SCSN as comparison. Our results are very consistent with the first-motion mechanisms and are quite sensitive to subtle changes in the mechanism, e.g., Sierra Madre aftershocks, Coso swarm. We have noticed that the solution is quite robust for errors in location of up to 10 km, which is the error level for the locations from the real-time system of SCSN. The time to obtain a solution, on the order of a minute, is a fraction of the time needed for data acquisition so that the next logical step for speeding up this process will be installation of continuous data transmission from the stations to the central site at the Caltech Seismo Lab.

The correction for lateral inhomogeneity of the crust works very well in most cases, but the amplitudes at SBC are persistently higher than predicted by our moment-tensor solutions. This is almost certainly due to strong multipathing and scattering in this area since the wave trains tend to have long codas. For this reason we usually omit SBC from the inversion until we have solved this problem, either by including some empirical correction or by using more sophisticated raytracing methods that take lateral velocity variations into account.

The number of stations needed to obtain a reliable solution depends on many factors like azimuthal coverage, mechanism, noise level, and accuracy of the velocity model. In many cases, we found that two stations can actually give good results, provided we can use both Love and Rayleigh waves. An example is the Coso swarm where we often had data from only GSC and ISA. The solutions, plotted in Figures 10a through 10f, vary from event to event. This variation is obvious in the solutions obtained from the first-motion data. This demonstrates that even with only two stations we can resolve the difference in the mechanisms shown in Figures 10a through 10f.

In Table 2, we compare the results of our work with body-waveform inversions on the Sierra Madre earthquake by Dreger and Helmberger (1991) and Wald (1992) as well as the Harvard CMT solution. Our mechanism is very similar to theirs; our moment, 3.3×10^{24} dyne-cm, is somewhat larger but comparable to their solutions. Likewise, our results for the Joshua Tree and Big Bear earthquakes are very similar to those of other studies (Tables 3 and 4). The difference in moment between the various authors can be attributed to the use of different crustal models, different depth, and different frequency range of the data used for the inversion. The solutions for the Sierra Madre mainshock and some of the aftershocks are plotted in Figures 10g through 10k. A comparison of this solution with the first motions clearly demonstrates that we can resolve subtle changes in mechanism.

The smallest event we could analyze was the Wrightwood event (Fig. 10l), which had a local magnitude of 3.2. This event was favorably located in the middle of TERRAscope with both good azimuthal coverage and short distances. For more general locations within the TERRAscope network the magnitude of the smallest event we can analyze is about 3.4, but with the increasing number of stations we expect that an M_W of 3.0 will be our lower limit for routine processing.

An upper limit to the size is primarily set by the dimensions of the rupture since we are using a point-source approximation. We could not obtain a satisfactory solution for the Landers ($M_W = 7.3$) earthquake because of strong directivity and large source dimensions. However, the Joshua Tree ($M_W = 6.1$) and the Big Bear earthquakes ($M_W = 6.4$) were still within the capability of our method.

The Joshua Tree and Landers sequences (Kanamori *et al.*, 1992; Hauksson *et al.*, 1993) provided a wealth of data for testing our method. The focal mechanisms we determined are plotted in Figures 11 and 12 for selected regions. The aftershocks have a wide range of mechanisms. Many of them are very different from the mainshock mechanism. In fact, some of the larger aftershocks to the Landers and Big Bear earthquakes are purely dip-slip. Because of the data-retrieval system at the time, most of these solutions were obtained within half an hour after the events occurred, which means that we did run up a small backlog of events in the very early stages of the aftershock sequence, but not thereafter.

Although a good azimuthal station coverage is desirable, we are not restricted to events that are within the TERRAscope area. We have included several outlying events like the San Simeon (central California), San Miguel (Baja California), Little Skull Mountain (Nevada), Alum Rock (near San Jose), and Parkfield earthquakes. Because of the larger

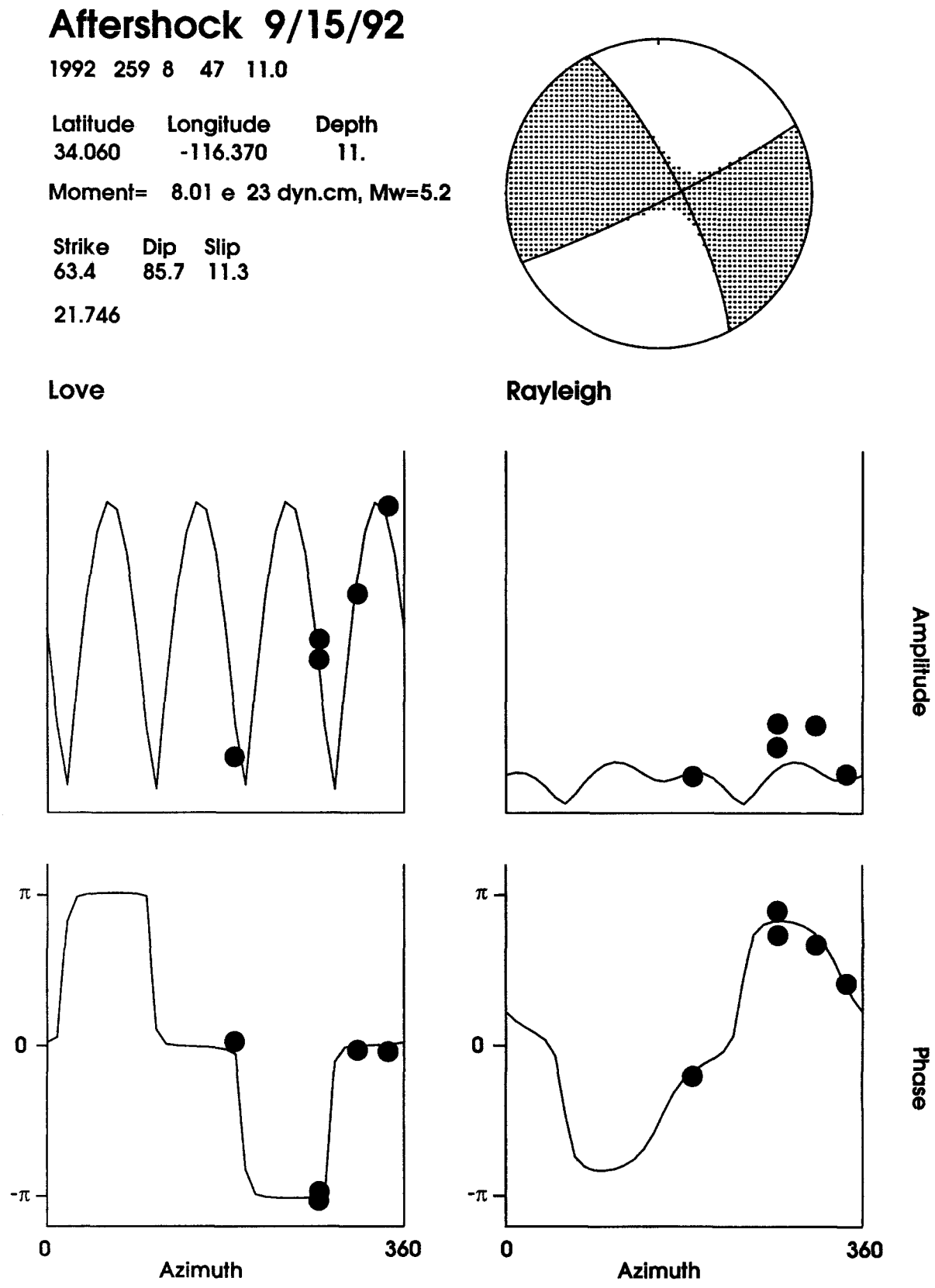

Figure 9. Moment-tensor solution for an aftershock to the Landers earthquake (same as in Fig. 8). In the lower panel, the azimuthal variation of the source spectrum (at 20 sec) is plotted. The dots represent observed values, the lines are theoretical values corresponding to the mechanism given.

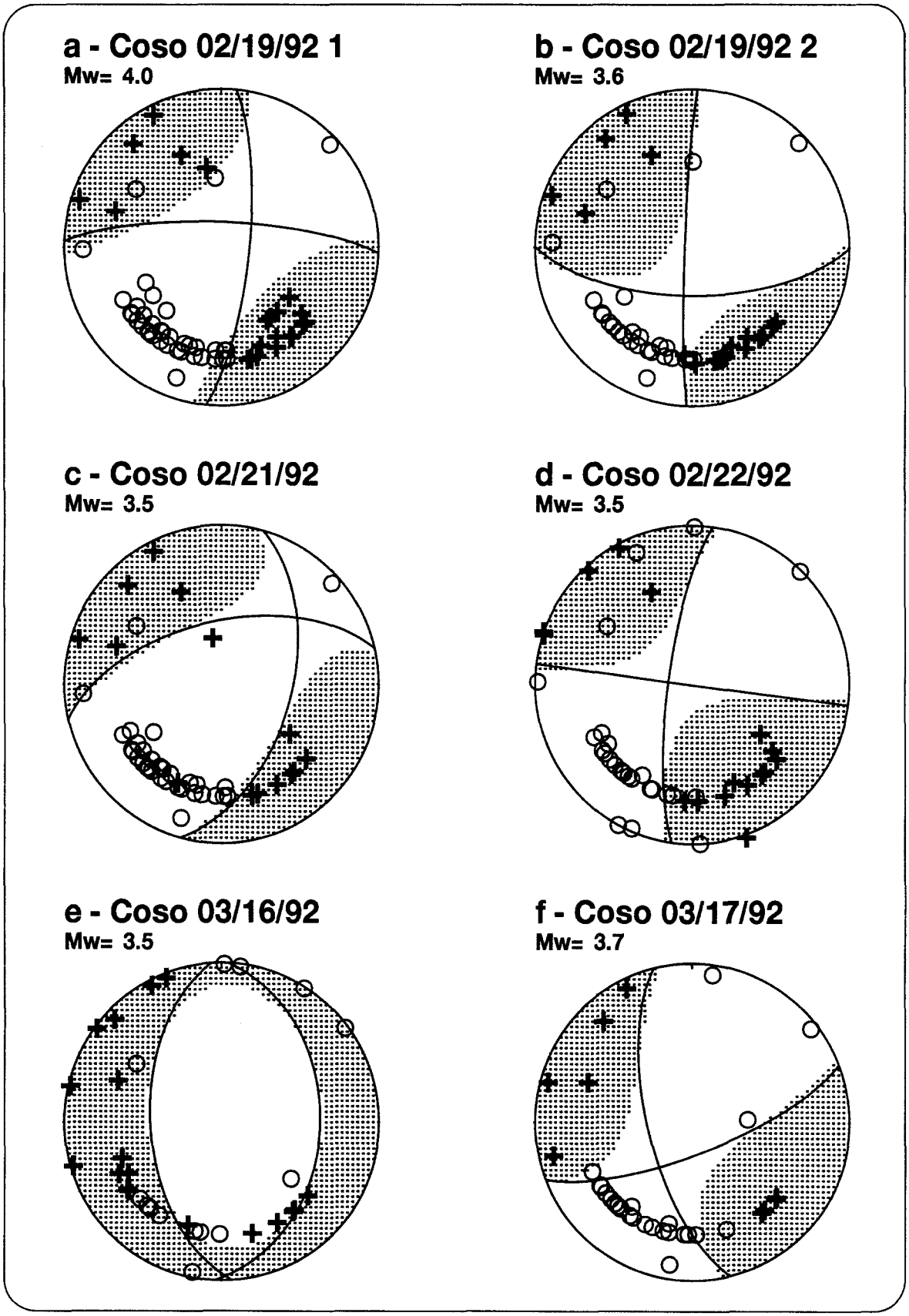

Figure 10. A comparison of our moment-tensor solution solutions and first-motion data from the SCSN. (a) through (f) Coso swarm (Feb/March 1992), (g) through (k) Sierra Madre sequence, (l) Wrightwood.

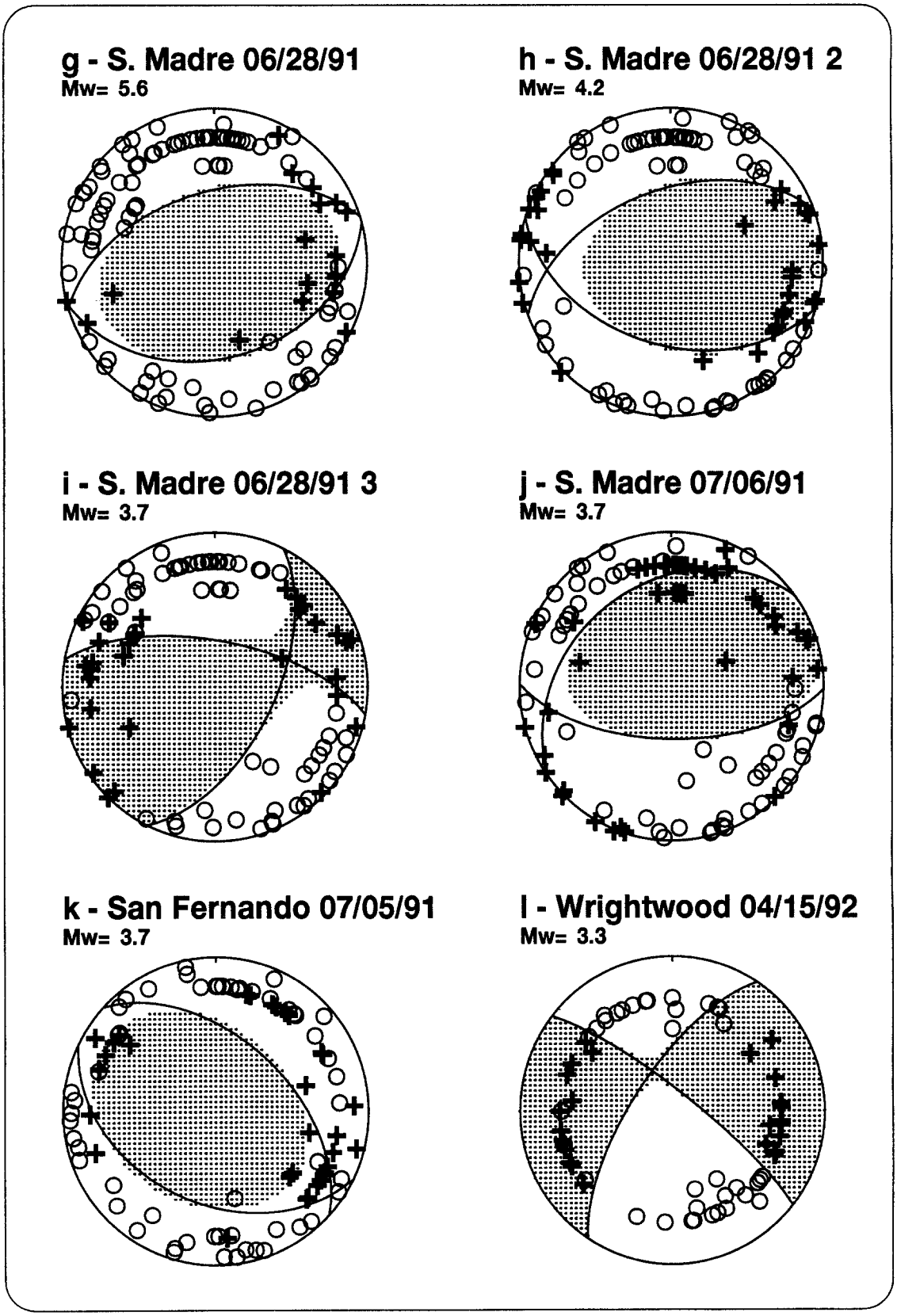

Figure 10—*Continued*

Table 2

Comparison of Results for the Sierra Madre Earthquake. DH—Dreger and Helmberger, 1992; Wald—Wald, 1992; Harvard—Dziewonski *et al.*, 1992.

	Strike	Dip	Slip	Moment	Depth
DH	235.0	50.0	74.0	2.5	12.0
Wald	243.0	49.0	82.0	2.8	11.0
Harvard CMT	223.0	58.0	58.0	3.6	15.0
This study	253.0	52.0	89.0	3.3	11.0

Table 3

Comparison of Results for the April 1992 Joshua Tree Earthquake. Dreger—D. Dreger (personal comm.); Harvard—Dziewonski *et al.*, 1993.

	Strike	Dip	Slip	Moment	Depth
Dreger	263.0	73.0	2.0	1.43	11.0
Harvard CMT	81.0	87.0	−1.0	3.6	15.0
This study	83.0	78.0	6.0	1.95	10.0

Table 4

Comparison of Results for the June 1992 Big Bear Earthquake. JH—Jones and Hough, 1993; Harvard—Dziewonski *et al.*, 1993.

	Strike	Dip	Slip	Moment	Depth
JHH	321.0	86.0	200.0	5.3	3–8
Harvard CMT	48.0	88.0	2.0	6.78	15.0
This study	46.0	81.0	7.0	4.52	12.0

distances the influence of lateral inhomogeneity is more severe, especially at shorter periods. Hence, we generally choose longer periods (up to 60 sec) for these events. The resulting source mechanisms for these events are consistent with other studies [Dreger and Helmberger, 1993 (San Miguel); Walter, 1993 (Little Skull Mountain); Ritsema, personal comm. (Parkfield); and Pasyanos, personal comm. (Alum Rock)].

Another advantage of our method is that we now obtain reliable estimates of seismic moments on a routine basis for events down to magnitude 3. Comparison of these values with estimates of seismic energy and with the local magnitudes provides a basis for scaling relations for earthquakes in southern California. In Figure 13, we compare the seismic moments with the local magnitudes determined with SCSN short-period data. The dominant frequency in the M_L determinations is 1 Hz, whereas our seismic moments are estimated at periods longer than 10 sec. The relationship between log M_0 and M_L is linear over the whole range from M_L = 3 to 6.5. The best fit is M_L = (log (M_0) − 16.1)/1.5, which is the relation found by Thatcher and Hanks (1973). The scatter is less for earthquakes in the 6- to 10-km-depth range than for other depth ranges that may be the result of higher mode contamination and lateral heterogeneity.

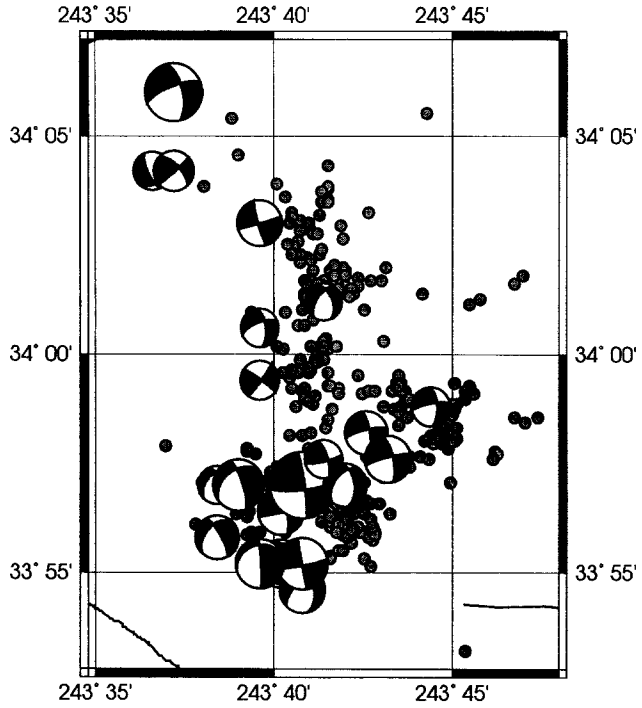

Figure 11. Focal mechanisms for events from the Joshua Tree sequence.

Kanamori *et al.* (1993) found a linear relationship between log E_S (E_S: released energy) and M_L with a slope of 1.96. This and the slope of 1.5 of the log M_0 versus M_L relationship suggests $E_S/M_0 \sim M_0^{1/3}$ on the average.

Conclusions

Short-period surface waves can be used for routine moment-tensor determinations of local earthquakes with magnitude greater than 3.2. In combination with the real-time location provided by the SCSN, this method can be automated for real-time mechanism and moment determinations. Since this inversion does not require any manual processing except perhaps for eliminating noisy records, in the case of smaller events, it is very straightforward to automate this process and include it in the routine automatic analysis performed at the SCSN. The system can be further refined by allowing for finite rupture and by including a grid-search technique to determine better locations in case the RTP location is not accurate enough. Our results confirm the results obtained by Thatcher and Hanks (1973) on the relationship between M_0 and M_L.

Acknowledgments

We would like to thank the people responsible for the daily operation of the Southern California Seismic Network for their help. This work was partially supported by USGS Grant Number 1434-93-G-2287. Division of Geological and Planetary Sciences Contribution Number 5467.

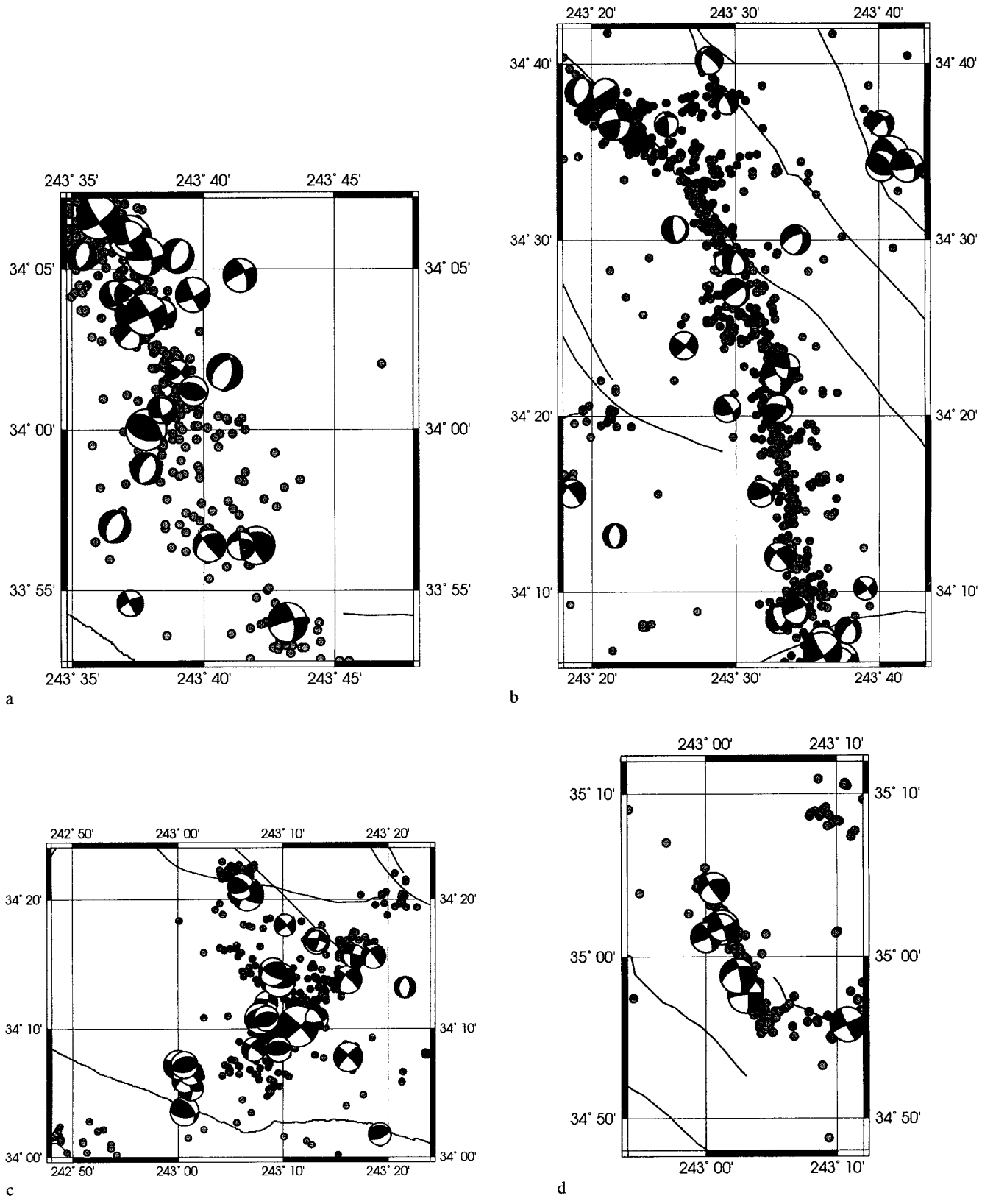

Figure 12. Focal mechanisms for events from the Landers–Big Bear sequence, (a) same region as Figure 8, (b) the Landers rupture zone, (c) the Big Bear area, and (d) the Barstow area.

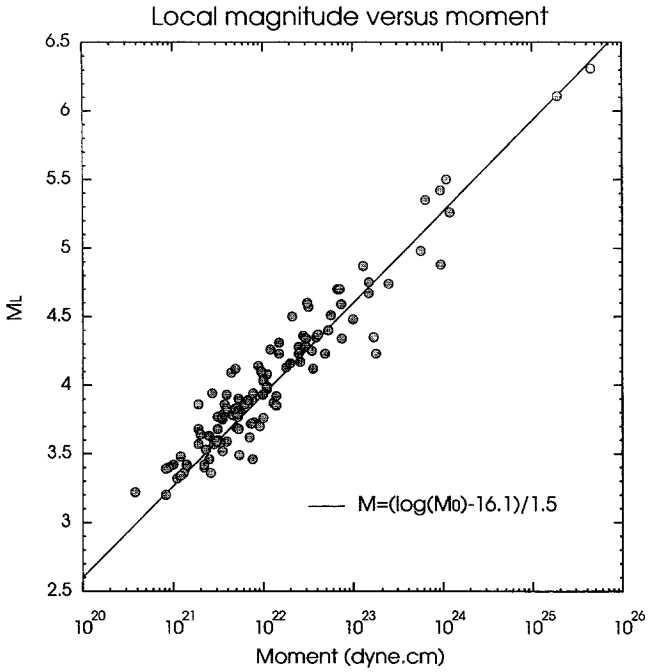

Figure 13. Relationship between seismic moment (M_0) and local magnitude (M_L). The solid line represents the relation $M = (\log(M_0) - 16.1)/1.5$.

References

Aki, K. (1966). Generation and propagation of G waves from the Niigata earthquake of June 16, 1964. Part 2. Estimation of earthquake moment, released energy and stress-strain drop from the G wave spectrum, *Bull. Earthquake Res. Inst.* **44,** 73–88.

Dreger, D. and D. H. Helmberger (1991). Source parameters of the Sierra Madre earthquake from regional and local body waves, *Geophys. Res. Lett.* **18,** no. 11, 2015–2018.

Dreger, D. and D. H. Helmberger (1993). Determination of source parameters at regional distances with three-component sparse network data, *J. Geophys. Res.* **98,** no. B5, 8107–8125.

Dziewonski, A. M. and J. H. Woodhouse (1983). Studies of the seismic source using normal-mode theory, in *Earthquakes: Observation, Theory and Interpretation,* H. Kanamori and E. Boschi (Editors), 45–137. North-Holland: Amsterdam, The Netherlands.

Dziewonski, A. M., G. Ekström, and M. P. Salganik (1992). Centroid moment tensor solutions for April-June 1991, *Phys. Earth Planet. Interiors* **71,** 6–14.

Dziewonski, A. M., G. Ekström, and M. P. Salganik (1993). Centroid moment tensor solutions for April-June 1992, Phys. Earth Plan. Interios **77,** 151–163.

Hauksson, E., L. M. Jones, K. Hutton, and D. Eberhart-Phillips (1993). The 1992 Landers earthquake sequence: seismological observations, *J. Geophys. Res.* **98,** (B11), 19,835–19,858..

Jones, L. E. and S. E. Hough (1993). Analysis of broadband records from the June 28, 1992 Big Bear earthquake: evidence of a multiple-event source, *Bull. Seism. Soc. Am.* in press (1995).

Kanamori, H. and J. W. Given (1981). Use of long-period surface waves for rapid determination of earthquake-source parameters, *Phys. Earth Planet. Interiors* **27,** 8–31.

Kanamori, H., H. K. Thio, D. Dreger, E. Hauksson, and T. H. Heaton (1992). Initial investigation of the Landers, California, earthquake of 28 June 1992 using TERRAscope, *Geophys. Res. Lett.* **19,** no. 22, 2267–2270.

Kanamori, H., J. Mori, E. Hauksson, T. H. Heaton, L. K. Hutton, and L. M. Jones (1993). Determination of earthquake energy release and M_L using TERRAscope, *Bull. Seism. Soc. Am.* **83,** no. 2, 330–346.

Kawakatsu, H. (1989). Centroid single force inversion of seismic waves generated by landslides, *J. Geophys. Res.* **94,** 12363–12374.

Mendiguren, J. A. (1977). Inversion of surface wave data in source mechanism studies, *J. Geophys. Res.* **82,** 889–894.

Patton, H. J. (1980). Reference point method for determining the source and path effects of surface waves, *J. Geophys. Res.* **85,** 821–848.

Patton, H. J. and G. Zandt, (1991). Seismic moment tensors of western U.S. earthquakes and implications for the tectonic stress field, *J. Geophys. Res.* **96,** no. B11, 18245–18259.

Ritsema, J. and T. Lay (1993). Rapid source mechanism determination of large ($M_W \geq 5$) earthquakes in the western United States, *Geophys. Res. Lett.* **20,** no. 15, 1611–1614.

Romanowicz, B. and T. Monfret (1986). Source process times and depths of large earthquakes by moment tensor inversion of mantle wave data and the effect of lateral heterogeneity, *Ann. Geophys.* **4,** 271–183.

Romanowicz, B., D. Dreger, M. Pasyanos, and R. Uhrhammer (1993). Monitoring of strain release in central and northern California using broadband data, *Geophys. Res. Lett.* **20,** no. 15, 1643–1646.

Thatcher, W. and T. C. Hanks (1973). Source parameters of southern California earthquakes, *J. Geophys. Res.* **78,** 8547–8576.

Wald, D. J. (1992). Strong-motion and broadband teleseismic analysis of the 1991 Sierra Madre, California, earthquake, *J. Geophys. Res.* **97,** no. B7, 11033–11046.

Walter, W. R. (1993). Source parameters of the June 29 Little Skull Mountain earthquake from complete regional waveforms at a single station, *Geophys. Res. Lett.* **20,** no. 5, 403–406.

Appendix A

Moment-tensor solutions for the years 1990 through 1993. Epicentral coordinates, origin times, and local magnitudes (M_L) were supplied by the Southern California Seismic Network. An up-to-date list of these solutions is accessible via the World Wide Web with the following link: "http://www.gps.caltech.edu/terrascope/TerraMech.html".

Date (m/d/yr)	Time	M_0		M_W	M_L	Strike	Dip	Rake	Lat.	Long.	Dep.
			Exp.								
12/17/90	17:44:21.2	2.4	21	3.5		−154.	56.	11.	34.21	−117.02	
12/18/90	16:56:43.0	1.1	22	4.0		15.	81.	10.	35.37	−118.85	15.
06/28/91	14:43:54.3	3.3	24	5.6		253.	52.	89.	34.26	−118.00	11.
06/28/91	15:37:58.8	4.1	21	3.7		27.	58.	29.	34.25	−117.98	20.
06/28/91	17:00:55.0	2.7	22	4.2		−110.	51.	65.	34.26	−118.00	10.
06/29/91	17:53:52.0	4.0	21	3.7		−115.	68.	−3.	34.91	−116.58	
07/05/91	17:41:57.1	4.8	21	3.7		−47.5	51.	101.	34.50	−118.55	10.

Appendix A—*Continued*

Date (m/d/yr)	Time	M_0	Exp.	M_w	M_L	Strike	Dip	Rake	Lat.	Long.	Dep.
07/06/91	22:54:39.0	3.8	21	3.7		−126.	33.	58.	34.24	−118.00	
09/17/91	21:10:29.0	1.9	23	4.8		−60.	60.	125.	35.82	−121.33	4.
10/12/91	14:39:32.1	1.1	22	4.0		−109.	75.	−29.	33.89	−116.16	8.
10/27/91	20:54:05.8	1.8	21	3.4		−61.	37.	119.	33.67	−116.74	11.
12/03/91	17:54:37.0	8.4	23	5.2		25.	76.	350.	31.81	−115.81	15.
12/04/91	07:10:57.0	8.9	21	3.9		−111.	89.	3.	33.07	−116.80	
12/04/91	08:17:03.0	4.2	21	3.7		61.	73.	31.	34.18	−117.02	11.
12/20/91	10:38:29.0	8.9	21	3.9		−124.	60.	−14.	35.54	−117.35	7.
02/19/92	11:19:24.0	7.0	21	3.8		7.	67.	204.	36.03	−117.88	2.
02/19/92	12:24:39.9	2.6	21	3.5		−179.	88.	−152.	36.03	−117.88	4.
02/22/92	03:32:20.0	1.9	21	3.5	3.86	−173.	74.	178.	36.06	−117.82	5.
02/21/92	04:17:54.0	2.0	22	3.5		−103.	56.	−41.	36.01	−117.90	4.
03/03/92	08:07:48.4	3.1	21	3.6	3.77	178.	30.	149.	35.77	−118.03	7.
03/04/92	19:06:27.0	1.6	22	4.1		−99.	50.	56.	32.96	−118.80	
03/05/92	18:24:22.8	3.9	21	3.7	3.83	−107.	38.	82.	35.22	−119.37	23.
03/17/92	11:56:35.0	4.6	21	3.7	3.78	74.	89.	347.	36.00	−117.88	5.
04/10/92	20:13:23.0	4.0	21	3.7		−79.	54.	141.	33.39	−116.31	
04/15/92	19:05:47.2	1.0	21	3.3	3.42	−146.	69.	−11.	34.29	−117.57	7.
04/23/92	02:25:30.1	3.1	22	4.3	4.60	76.	86.	20.	33.94	−116.33	12.
04/23/92	04:50:22.9	1.9	25	6.1	6.11	83.	78.	6.	33.95	−116.32	10.
04/23/92	13:35:58.1	1.0	22	3.9		−115.	52.	−13.	33.92	−116.32	4.
04/23/92	18:06:41.9	3.3	21	3.6		87.	85.	7.	33.94	−116.30	13.
04/23/92	18:20:13.0	4.0	21	3.7		−120.	69.	−34.	34.03	−116.33	4.
04/23/92	18:56:03.0	1.1	22	4.0	4.08	−104.	77.	−14.	33.97	−116.29	6.
04/23/92	22:55:56.9	3.5	21	3.6	3.76	36.	85.	4.	33.99	−116.34	13.
04/23/92	23:52:40.0	3.5	21	3.6	3.75	−101.	75.	−28.	33.98	−116.26	4.
04/24/92	03:29:59.0	2.3	21	3.5	3.53	−111.	65.	−30.	34.01	−116.34	4.
04/25/92	09:34:41.0	5.3	21	3.8	3.68	−110.	78.	−22.	33.95	−116.30	7.
04/26/92	03:07:57.0	1.9	21	3.4	3.68	−147.	56.	−50.	34.02	−116.31	15.
04/26/92	06:26:08.0	4.9	22	4.4	4.23	−114.	50.	−21.	33.92	−116.33	4.
04/26/92	17:21:38.0	2.5	22	4.2	4.28	74.	89.	354.	34.05	−116.34	8.
04/27/92	03:11:19.0	2.6	22	4.2	4.17	−134.	62.	−51.	33.91	−116.32	4.
04/28/92	11:13:20.6	7.9	21	3.9	3.73	−151.	48.	−71.	33.92	−116.32	5.
04/28/92	11:33:27.0	1.3	22	4.0	3.87	−143.	47.	−56.	33.95	−116.30	4.
04/30/92	01:50:44.0	5.0	21	3.7	3.69	−101.	55.	−19.	34.02	−116.09	5.
05/01/92	13:38:42.5	5.2	21	3.7	3.79	−140.	39.	−69.	33.92	−116.33	10.
05/02/92	12:46:42.0	4.4	21	3.7	4.09	70.	89.	330.	33.99	−116.41	5.
05/02/92	19:10:24.1	2.2	21	3.5	3.40	76.	80.	18.	33.96	−116.31	9.
05/04/92	01:16:02.4	1.1	22	4.0	3.97	−138.	43.	−24.	33.93	−116.36	9.
05/04/92	16:19:49.9	1.5	23	4.7	4.75	79.	84.	359.	33.92	−116.32	12.
05/06/92	02:38:43.0	7.4	22	4.5	4.59	−104.	24.	−12.	33.92	−116.34	10.
05/12/92	02:31:29.0	3.9	22	4.3	4.35	−105.	83.	−20.	33.96	−116.28	9.
05/18/92	00:22:34.0	2.5	21	3.5	3.46	−135.	40.	−30.	33.95	−116.36	11.
05/18/92	15:44:17.8	1.3	23	4.7	4.87	−126.	40.	−23.	33.95	−116.35	
05/31/92	10:53:16.0	6.0	20	3.1		−114.	59.	2.	34.59	−116.82	13.
05/31/92	11:38:45.0	1.8	21	3.4		−101.	63.	12.	34.57	−116.85	13.
06/28/92	12:36:41.0	1.2	24	5.3	5.26	−112.	72.	−28.	34.10	−116.38	16.
06/28/92	14:43.22.0	9.4	23	5.2	5.42	−76.	37.	130.	34.16	−116.85	11.
06/28/92	15:05:30.0	4.5	25	6.4	6.31	46.	81.	7.	34.17	−116.81	12.
06/28/92	17:48:32.0	3.0	22	4.3	4.28	−144.	57.	−12.	34.23	−116.73	7.
06/28/92	19:42:16.0	3.1	21	3.6	3.6	2.	81.	142.	34.00	−116.50	1.
06/28/92	20:23:19.0	2.2	21	3.5	3.42	156.	69.	−124.	34.07	−116.39	26.
06/28/92	22:13:11.0	5.3	21	3.7	3.90	48.	86.	25.	34.07	−116.38	9.
06/29/92	10:14:22.0	2.8	24	5.6		179.	36.	−135.	36.60	−116.30	12.
06/29/92	14:08:38.0	2.3	23	4.8		61.	60.	2.	34.11	−116.40	21.
06/29/92	14:13:38.0	1.1	24	5.3		56.	71.	352.	34.11	−116.40	17.
06/29/92	14:31:30.0	2.1	22	4.2	4.5	−165.	57.	−103.	34.09	−116.35	8.
06/29/92	14:41:26.0	8.3	22	4.5		−158.	76.	−5.	34.12	−117.00	11.
06/29/92	16:01:43.0	2.0	24	5.5		70.	85.	19.	33.86	−116.30	7.
06/29/92	19:10:31.0	5.1	21	3.7		−98.	89.	8.	33.85	−116.29	11.
06/29/92	22:52:16.0	9.1	21	3.9	3.70	92.	52.	15.	34.17	−118.18	1.
06/30/92	00:23:56.0	4.0	21	3.7		152.	63.	−134.	34.14	−116.45	10.

Appendix A—*Continued*

Date (m/d/yr)	Time	M_0	Exp.	M_w	M_L	Strike	Dip	Rake	Lat.	Long.	Dep.
06/30/92	05:33:47.0	5.9	21	3.8		−138.	44.	−12.	34.26	−116.69	10.
06/30/92	11:30:29.0	1.5	22	4.0	4.31	73.	87.	10.	34.07	−116.45	18.
06/30/92	12:14:50.0	9.5	21	3.9	4.1	45.	81.	356.	34.05	−116.47	16.
06/30/92	12:26:19.0	3.9	21	3.7	3.59	−131.	78.	−35.	34.01	−116.36	4.
06/30/92	12:34:55.0	4.9	21	3.7	4.12	−51.	43.	143.	34.26	−116.47	4.
06/30/92	13:05:36.0	1.0	23	4.6	4.48	29.	88.	354.	35.68	−117.61	5.
06/30/92	14:38:11.0	5.7	23	5.1	4.98	−45.	43.	112.	34.00	−116.37	15.
06/30/92	17:26:30.0	1.2	22	4.0	4.26	−177.	53.	−108.	34.64	−116.68	5.
06/30/92	20:05:06.0	7.5	21	3.9	3.89	−154.	57.	−85.	33.98	−116.37	4.
06/30/92	21:22:54.0	6.7	22	4.5	4.70	−136.	81.	−7.	34.13	−116.73	7.
06/30/92	21:49:01.0	7.5	22	4.5	4.34	−42.	45.	125.	34.06	−116.99	1.
07/01/92	00:14:27.0	7.6	21	3.9	3.46	6.	81.	345.	34.09	−116.98	13.
07/01/92	17:45:52.0	1.1	22	4.0		−84.	66.	64.	33.93	−116.71	8.
07/02/92	05:16:34.0	4.9	21	3.7	3.83	76.	58.	26.	34.34	−116.51	6.
07/02/92	12:17:42.0	1.2	21	3.3	3.48	−112.	39.	165.	34.61	−116.58	11.
07/02/92	15:11:58.0	3.8	20	3.0	3.22	46.	71.	13.	34.03	−116.35	13.
07/02/92	18:53:51.0	1.5	21	3.4		−109.	42.	106.	34.05	−116.58	13.
07/02/92	22:25:27.0	8.8	21	3.9	4.14	36.	71.	358.	35.77	−117.59	7.
07/03/92	02:40:52.0	3.5	21	3.6	3.52	−60.	67.	107.	33.16	−115.65	11.
07/03/92	04:10:49.0	7.9	20	3.2		52.	78.	11.	34.17	−116.35	9.
07/03/92	04:15:51.0	2.7	21	3.6	3.94	78.	60.	215.	34.18	−116.78	15.
07/03/92	04:19:41.0	9.9	20	3.3		−175.	42.	−86.	34.22	−116.64	11.
07/03/92	05:55:43.0	8.3	20	3.2	3.20	69.	53.	345.	34.01	−116.36	2.
07/03/92	10:40:08.0	3.1	21	3.6	3.68	20.	86.	18.	34.20	−116.86	13.
07/03/92	11:40:28.0	1.2	21	3.3		−118.	75.	1.	33.91	−116.38	8.
07/03/92	12:32:24.0	8.8	20	3.2	3.40	−143.	35.	−33.	34.63	−116.51	7.
07/03/92	17:17:02.0	6.6	21	3.8		39.	81.	4.	34.40	−116.56	16.
07/04/92	09:36:01.0	1.4	21	3.4	3.42	51.	82.	10.	34.30	−116.83	19.
07/05/92	05:49:39.0	1.4	22	4.0	3.85	−154.	49.	−86.	33.95	−116.39	5.
07/05/92	10:36:19.0	2.6	21	3.5		131.	76.	−38.	34.61	−116.33	7.
07/05/92	10:55:45.0	3.2	22	4.3	4.57	−115.	80.	−9.	35.03	−116.98	9.
07/05/92	21:18:27.0	1.1	24	5.3	5.5	76.	72.	34.	34.58	−116.32	8.
07/05/92	22:33:47.0	3.5	22	4.3	4.25	−37.	50.	114.	34.57	−116.33	9.
07/06/92	12:00:58.0	2.8	22	4.2	4.36	−117.	82.	−29.	34.08	−116.31	8.
07/06/92	19:41:37.0	3.0	22	4.3	4.34	64.	78.	356.	34.07	−116.34	16.
07/08/92	02:23:10.0	7.1	22	4.5	4.70	79.	77.	36.	34.57	−116.30	8.
07/09/92	01:43:58.0	9.5	23	5.3	4.88	−123.	47.	61.	34.23	−116.84	1.
07/10/92	01:29:41.0	3.6	22	4.3	4.12	−120.	37.	37.	34.24	−116.85	1.
07/10/92	02:41:15.0	1.4	22	4.0	3.92	127.	89.	266.	34.12	−116.40	2.
07/10/92	16:01:38.0	1.2	21	3.3	3.34	23.	88.	219.	34.48	−116.51	12.
07/11/92	07:21:37.0	6.2	21	3.8		−124.	84.	−72.	34.45	−116.50	1.
07/11/92	18:14:17.0	6.7	23	5.1		−147.	86.	−32.	35.21	−118.07	24.
07/12/92	05:35:14.0	5.2	21	3.7	3.77	173.	72.	−97.	34.51	−116.57	4.
07/13/92	05:00:01.0	2.0	21	3.5	3.64	−175.	46.	−103.	34.09	−116.41	11.
07/14/92	20:36:52.0	7.0	21	3.8	3.62	−27.	6.	5.	34.64	−116.65	1.
07/15/92	00:18:57.0	5.5	21	3.8	3.81	28.	53.	28.	34.34	−116.45	3.
07/15/92	12:45:22.0	2.8	21	3.6	3.57	−140.	68.	−57.	34.13	−116.37	8.
07/20/92	04:08:24.0	7.7	21	3.9	3.94	−135.	60.	−6.	34.20	−116.45	8.
07/20/92	04:48:02.0	5.3	22	4.4	4.40	−98.	83.	−15.	34.96	−116.95	9.
07/20/92	13:13:21.0	5.7	22	4.4	4.51	−112.	53.	−17.	34.98	−116.96	3.
07/24/92	18:14:37.0	2.5	23	4.9	4.74	−105.	84.	−28.	33.90	−116.28	8.
07/24/92	07:23:57.0	3.7	21	3.6	3.86	−163.	65.	−59.	34.48	−116.50	15.
07/25/92	04:32:00.0	1.5	23	4.7	4.67	−99.	32.	21.	33.94	−116.30	8.
07/27/92	20:40:09.0	3.9	21	3.7	3.93	−138.	90.	29.	32.67	−115.62	2.
07/28/92	18:27:04.0	1.7	23	4.8	4.35	84.	76.	27.	34.09	−116.37	15.
08/04/92	19:06:12.0	1.0	22	3.9	3.76	64.	65.	345.	34.10	−116.38	3.
08/05/92	15:41:54.0	6.7	21	3.8	3.89	−165.	37.	−31.	34.67	−116.53	22.
08/08/92	15:37:43.0	2.5	22	4.2	4.23	−101.	71.	−15.	34.37	−116.45	7.
08/11/92	06:11:17.0	1.1	22	4.0	3.99	71.	67.	3.	34.06	−116.37	9.
08/15/92	18:18:05.0	5.4	21	3.8	3.49	−128.	73.	−12.	34.10	−116.99	4.
08/16/92	06:30:59.0	3.0	21	3.6	3.59	−86.	28.	115.	34.03	−116.68	11.
08/17/92	20:41:51.0	1.8	23	4.8	4.23	−102.	37.	107.	34.18	−116.87	15.

Appendix A—*Continued*

Date (m/d/yr)	Time	M_o	Exp.	M_w	M_L	Strike	Dip	Rake	Lat.	Long.	Dep.
08/18/92	09:46:40.0	9.9	21	3.9	4.08	−100.	51.	98.	34.18	−116.86	4.
08/23/92	06:40:44.0	6.2	21	3.8	3.86	67.	85.	22.	35.02	−117.00	8.
08/24/92	13:51:46.0	1.8	22	4.1	4.13	−113.	86.	−30.	34.28	−116.78	8.
08/24/92	18:21:42.0	8.3	20	3.2	3.39	14.	78.	11.	34.28	−116.78	6.
08/26/92	13:21:56.0	5.0	21	3.7		73.	75.	8.	34.06	−116.36	4.
08/26/92	13:50:48.0	1.1	21	3.3	3.32	−117.	55.	−7.	34.11	−116.98	5.
08/30/92	08:15:12.0	2.6	21	3.5	3.36	−61.	50.	70.	34.01	−118.36	10.
08/31/92	09:25:39.0	1.5	22	4.1	4.23	−115.	62.	−50.	34.50	−116.43	14.
09/03/92	06:17:38.0	2.5	21	3.5	3.63	2.0	76.	170.	34.38	−116.44	13.
09/05/92	03:29:27.0	3.6	21	3.6	3.79	35.	59.	18.	34.11	−116.40	9.
09/06/92	22:47:29.0	1.3	21	3.4	3.36	−128.	83.	−40.	35.03	−116.98	8.
09/08/92	03:44:49.0	6.5	21	3.8		−131.	65.	−2.	34.11	−116.98	7.
09/09/92	11:44:55.0	1.0	22	3.9	4.03	−119.	52.	8.	35.07	−116.99	2.
09/09/92	12:50:44.0	2.0	22	4.1	4.16	−127.	40.	4.	33.94	−116.33	8.
09/11/92	18:58:22.0	1.9	21	3.4	3.57	68.	87.	8.	35.03	−116.98	9.
09/15/92	08:47:11.0	8.0	23	5.2		63.	86.	11.	34.06	−116.37	11.
09/16/92	12:27:22.0	3.3	21	3.6	3.58	50.	85.	14.	34.06	−116.38	9.
09/18/92	12:53:35.0	7.3	21	3.8	3.72	−134.	80.	−47.	34.05	−116.38	8.
09/22/92	18:52:33.0	9.9	21	3.9	3.93	−134.	80.	−47.	34.05	−116.38	8.
10/02/92	07:19:57.0	4.2	22	4.4		−98.	72.	152.	34.61	−116.64	5.
10/11/92	12:38:13.0	4.1	22	4.3	4.37	−116.	88.	3.	34.93	−116.82	12.
10/20/92	05:28:09.0	5.7	22	4.4		52.	84.	349.	35.93	−120.47	13.
11/24/92	09:06:26.0	4.6	21	3.7		−150.	59.	−10.	34.14	−116.88	13.
11/25/92	02:40:25.0	4.3	21	3.7		−121.	82.	22.	35.04	−116.96	12.
11/25/92	07:50:35.0	9.7	21	3.9		−23.	29.	−179.	34.15	−116.43	2.
11/27/92	16:00:57.0	6.4	23	5.1	5.35	−146.	80.	24.	34.34	−116.89	3.
12/04/92	12:59:42.0	1.7	22	4.1		−50.	55.	137.	34.35	−116.90	1.
03/20/93	06:56:55.0	4.1	21	3.7		−176.	67.	−106.	34.01	−117.23	11.
04/29/93	08:21:01.0	1.1	24	5.3		−79.	73.	−96.	35.60	−112.10	8.
05/17/93	23:20:50.0	1.6	25	6.1		−173.	48.	−110.	37.20	−117.77	9.
05/18/93	23:48:55.0	4.1	23	5.0		84.	24.	13.	37.06	−117.76	5.
05/18/93	17:09:05.0	2.3	21	3.5		−76.	51.	80.	34.29	−117.48	12.
05/19/93	14:13:24.0	1.8	23	4.8		−179.	74.	−101.	37.14	−117.73	5.
05/20/93	20:14:14.0	1.4	23	4.7		33.	38.	347.	36.09	−117.69	1.
05/28/93	04:47:40.0	1.8	23	4.8		−149.	37.	−6.	35.13	−119.10	21.
05/31/93	08:55:30.0	2.4	22	4.2		−111.	42.	81.	34.12	−116.99	7.
07/26/93	21:29:49.0	2.1	21	3.5		−82.	52.	113.	33.99	−118.74	18.
08/11/93	05:48:20.0	7.7	22	4.5		132.	50.	−120.	37.52	−118.89	6.
08/11/93	22:33:04.0	1.9	23	4.8		−131.	83.	18.	37.31	−121.68	6.
08/21/93	01:46:38.0	6.2	22	4.5		−134.	46.	−60.	34.03	−116.32	15.
09/06/93	08:25:23.0	8.3	21	3.9		−88.	35.	99.	34.14	−116.84	7.
09/06/93	10:32:33.0	2.4	21	3.5		−156.	42.	−50.	36.00	−118.37	5.
09/06/93	22:30:15.0	6.1	21	3.8		21.	85.	2.	32.51	−115.41	3.
10/04/93	02:57:37.0	3.9	21	3.7		−68.	50.	100.	34.02	−116.34	4.
10/13/93	09:54:03.0	6.4	21	3.8		157.	42.	124.	34.82	−120.95	6.
10/18/93	21:49:46.0	1.3	23	4.7	4.04	−111.	69.	30.	31.98	−118.86	5.
10/21/93	14:37:12.0	5.6	21	3.8		170.	39.	−112.	36.18	−118.03	3.
10/22/93	16:30:53.0	3.6	21	3.6	3.72	9.	65.	182.	36.10	−117.94	6.
10/25/93	00:18:50.0	2.1	21	3.5		−159.	47.	−66.	34.92	−116.85	4.
11/04/93	00:36:54.0	7.7	20	3.2	3.45	−125.1	33.	−51.	33.81	−115.66	9.
11/14/93	12:25:35.0	2.0	23	4.8		51.	89.	341.	35.95	−120.51	14.
12/03/93	01:51:25.0	3.1	21	3.6	3.67	−171.	66.	166.	34.26	−116.72	19.

Seismological Laboratory
California Institute of Technology
Pasadena, California 91125

Manuscript received 28 March 1994.